Multi-objective micro-geometry optimization of gear tooth supported by response surface methodology.

Jakub A. Korta[a,b,*], Domenico Mundo[a]

[a] *University of Calabria*
Department of Mechanical, Energy and Management Engineering,
Ponte Pietro Bucci, Cubo 46C, 87036 Rende, Italy
[b] *AGH University of Science and Technology,*
al. A. Mickiewicza 30, 30-059 Krakow, Poland

Abstract

This paper shows the application of response surface methodology for gear optimization using micro-geometry profile modifications. The suitability of three distinct metamodeling techniques is studied in this paper: Gaussian Process (stochastic), Shepard k-Nearest (nonparametric deterministic) and Polynomial (parametric deterministic). The described optimization strategy is implemented and tested on a case study consisting of a pair of identical spur gears, in which the goal is to find optimal micro-geometry modifications of tooth profile, providing decreased values of peak-to-peak transmission error and maximal contact stress along the meshing cycle, while maintaining the safety coefficient linked to tooth bending fatigue above a required threshold. The gear pair is analyzed under three different loading scenarios. It is shown that the described optimization strategy allows finding optimal micro-geometry modifications of tooth profile that enable significant improvements in all the observed performance indices with respect to the unmodified gear design, as confirmed by detailed numerical simulations of the optimal gears.

Keywords: gears, optimization, micro-geometry, mechanical transmission, response surface, transmission error

1. Introduction

With the development of numerical simulation methods, gear structural optimization has gained much attention by mechanical engineers, since computer - based analyses allow selecting an optimal design solution from a vast number of trial models, with limited need for costly and time consuming physical prototyping and testing. In order to improve gear operating parameters, tooth

*Corresponding author
Email addresses: jakub.korta@unical.it (Jakub A. Korta), domenico.mundo@unical.it (Domenico Mundo)

micro-geometry is often tuned to ameliorate the meshing process by eliminating flank-tip contact and, consequently, allowing loaded teeth for a smooth changeover. Currently, these issues are most frequently approached by using Finite Element Method (FEM) simulations, which can cover all the aspects of gear shape, position and operating conditions [1].

However, although the principles governing gears operation are well established and understood, detailed numerical analyses aimed at predicting their dynamic behavior and durability are still cumbersome and time consuming. This is because high fidelity approaches to gear numerical simulations require accurate description of local (i.e., contact stress) and global (i.e., tooth and body deflections) phenomena, which simultaneously influence the overall transmission behavior.

When it comes to optimization, it is commonplace to carry out these tasks by using analytical, semi-analytical or FE-based gear models. Artoni et al. [2] presented optimization methodology for cylindrical gears, based on micro-geometry modification of tooth, evaluating peak value of contact stress and peak-to-peak value of loaded transmission error (TE). Harianto and Houser [3] described a method for assessing the influence of gear geometry modification on various performance indices, including tooth root and contact stress and gear noise and vibration. Artoni et al. in ref. [4], described tooth geometry optimization in hypoid gears based on generalized tooth flank description, using the so-called ease-off parameterized surface. Bonori et al. [5] presented an implementation of genetic algorithms for spur gear optimization, aiming at minimizing the generated vibrations. The goal of the procedure was to decrease the peak-to-peak value of static transmission error (STE) using tip and root reliefs. As shown by Parker et al. [6], STE, which is simpler to calculate, can be used to predict gear dynamic behavior. According to the findings described by Cai in ref. [7], STE is strongly correlated with gear dynamics. Therefore, minimization of the peak-to-peak STE results in improvements of gear vibration behavior.

The optimal value of micro-geometry modifications is strongly correlated with the operational conditions, for which the transmission is designed. In other words, tip and root reliefs, which are optimal for a given loading torque, can perform worse than non-modified profile under a different load. Indeed, Faggioni et al. [8] used tooth profile modifications to perform a global optimization of gear vibrations in a wide range of operating conditions. A study on tooth profile modification was also discussed by Fernández et al. [9]. The authors took under consideration profile reliefs and manufacturing inaccuracies, showing their influence on the STE peak-to-peak values.

In case of simulation data that is difficult or long to predict and collect, the response surface methodology (RSM) can be usefully employed. This approach, which was studied extensively in the last decades, is based on the idea of substituting complex mathematical models by simpler, easy to compute representations that allow to predict the observed quantity values (i.e., the dependent variables) as a function of certain independent variables. In the result, a so-called surrogate or metamodel is generated, referred sometimes to as a 'model of a model'. A parameterized approximating function can be determined a pri-

ori (e.g., polynomial model) or not considered at all (e.g., Gaussian Processes or k-Nearest approaches), depending on the chosen algorithm. The latter alternative is perceived as more general and is often used when the output data exhibits a high degree of non-linearity or its form is simply unknown. The implementation of RSM to time consuming engineering optimization problems can be found in [10, 11]. A description of various variants of surrogate-based data approximation was presented in [12, 13].

Despite its great popularity in engineering, the RSM implementation to gear design, specifically to micro-geometry optimization, has gained scant popularity. Very limited information on its application is available in the literature dedicated to mechanical transmissions. One example can be found in ref. [14] by Zhang et al., in which Kriging method combined with Latin Hypercube Sampling (LHS) design of experiment (DoE) was used successfully to predict strength responses of large scale gears. Surrogates were used in this work to perform global optimization with genetic algorithms (GA), finding an optimal set of macro-geometrical parameter values. The authors emphasized the significance of metamodeling to simplify engineering problems which, due to detailed numerical simulations, are becoming increasingly time-demanding nowadays. Kayabasi and Erzincanli in ref. [15] used polynomial-based RSM to perform shape optimization of a harmonic drive. Other examples of using RSM can be found in [16, 17], in which data approximation techniques support optimization of gear manufacturing, aimed at improving the process of tooth profile generation. Zhang and Guo in [16] used second order polynomial regression to predict dynamic transmission error fluctuations calculated using an analytical model of planetary gearbox. Park in [17] used the same type of polynomial approach to predict variation of a static transmission error computed for helical gears.

Limited number of literature positions on the subject of RSM-based gear optimization can be identified as an open research gap and allows to pose a question on usefulness of metamodeling in this class of structural optimization problems. This paper aims at providing an insight into this issue and demonstrates the applicability of metamodel-based multi-objective gear optimization on a real-life case study. The RSM-based optimization was carried out on a pair of identical spur gears to obtain improvements in STE and contact stress, with a constraint on the fatigue safety coefficient for tooth bending. Each gear design was altered by micro-geometry modification and assessed by non-linear static FEM simulations. Three different metamodeling techniques were used to build the surrogates for every output quantity, namely: Gaussian Processes (GP), 3rd order polynomial model (PL) and Shepard k-Nearest (SKN). Each of the response surfaces was validated and the selected, most accurate metamodels were used in conjunction with multi-objective genetic algorithm (GA) in order to find a set of parameter values for optimal microgeometry modification. To make the optimization attempt more comprehensive, the objectives were settled for three different loading torque values: 350Nm, 500Nm and 650Nm.

The paper is structured as follows: Section 2 explains the idea of multi-objective optimization and discusses the use of population-based metaheuristics for solving this type of problems. Selected metamodeling techniques and

response surface validation indices are introduced to the reader in Section 3. Section 4 presents the RSM-based optimization process workflow. The concept of micro-geometry modifications are described in Section 5. Section 6 describes the case study numerical model used for FEM simulations and discusses the observed output quantities. Section 7 presents the generated metamodels and provides details on assessment of the accuracy for different data approximation methods. Section 8 presents the optimization assumptions and describes the relationships between the goals of the procedure. Section 9 presents the obtained surrogate-based quasi-optimal solutions and their numerical validation. Section 10 concludes the paper.

2. Multi-objective optimization

Following Coello et al. [18], a multi-objective optimization problems (MOP) can be defined by Eq. 1:

$$\begin{aligned} Objective: \quad & min/max[f(\mathbf{x})], \quad \mathbf{x} \in \Omega \\ Subject\ to: \quad & h_i(\mathbf{x}) = 0,\ g_j(\mathbf{x}) \leq 0, \\ & i = 1, ..., l,\ j = 1, ..., t \end{aligned} \tag{1}$$

where $f(\mathbf{x}) = [f_1(\mathbf{x}), ..., f_k(\mathbf{x})]$ is a vector of k objective functions, subject to l equality $h_i(\mathbf{x}) = 0, i = 1, ..., l$ and t inequality $g_j(\mathbf{x}) \leq 0, j = 1, ..., t$ constraints. An MOP solution minimizes or maximizes the components of $f(\mathbf{x})$ vector by modification of the design parameters $\mathbf{x} = [x_1, ..., x_n]$, defined on the problem design space Ω, i.e., $\mathbf{x} \in \Omega$. The solution to MOP is the so-called trade-off, also referred as Pareto-optimal design, representing a compromise between the possible improvements in separate objectives, as described by Artoni et al. [4].

2.1. Optimum-search algorithm

Population-based meta-heuristics and specifically genetic algorithms are a frequent choice as MOP solving method. The principal advantage of these meta-heuristics over deterministic methods is that they can be successfully implemented for finding a global optimum also in non-linear problems. This is because these methods are not based on gradient calculation and depart from multiple initial points, spread out in the design domain.

The state-of-the-art description of evolutionary algorithms, including GAs, can be found in ref. [18]. One of the most known genetic algorithm is the Non-Dominated Sorting GA II (NSGA-II), described by Deb et al. [19], which has been successfully used to solve a number of multi-objective structural optimization problems, e.g. [20, 21]. A modern variant of the NSGA-II algorithm is the controlled elitist GA (CEGA) [22], which allows progressing to a next generation also individuals which are not ranked as non-dominated, providing that their promotion results in maintaining a widely spread search region. This feature precludes premature convergence to a local optimum, increasing chances for finding genuinely global Pareto front.

2.2. Design of Experiment

In order to be able to span the response surface over the design domain, firstly a set of data points must be generated. These known values are used by the chosen RS algorithm for response model fitting, i.e., they provide information essential for data prediction. The test points can be chosen randomly, but more often their selection is driven by predefined principles that enable the design of experiment (DoE). The reason for this is to use as few test points as possible to explore the design domain in the most comprehensive manner.

A common choice of a DoE algorithm, which allows understanding higher order relationships between the independent and the dependent variables, is Latin Hypercube Sampling (LHS) [23]. Its main advantages over a random sample selection is that the LHS method divides each of design variable h into N equal-probability intervals, creating a grid of N^h subdomains. Next, a sample is randomly laid in each interval, creating a relatively uniformly distributed sample map, which is important for subsequent metamodeling. As a consequence, there are no excessively large areas in the design domain, for which no testing points are determined. Moreover, unfavorable sample clustering is avoided, saving computational time and effort.

3. Response Surface Modeling

As described in the introductory section, the RSM technique is used to find simple mathematical description of highly complex models which are analyzed in the design process. This substitution results in substantial improvement in computational efficiency, which is essential when detailed, high-fidelity models are utilized for numerical simulations. The following metamodeling techniques are discussed in this paper: polynomial model (P), Shepard k-Nearest (SKN) and Gaussian Process (GP).

3.1. Polynomial models

The polynomial metamodeling technique is parametric and deterministic, i.e., it requires a priori determination of underlying approximation model and specification of certain values of its parameters [13]. The general form of a third order function used in the subsequent study, takes the form of Eq. 2:

$$f(\mathbf{x}) = \beta_0 + \sum_{i=1}^{k} \beta_i x_i + \sum_{i=1}^{k} \sum_{j=1, i<j}^{k} \beta_{ij} x_i x_j + \sum_{i=1}^{k} \beta_{ii} x_i^2 + \\ + \sum_{i=1}^{k} \sum_{j=1, i<j}^{k} \beta_{ij} x_i^2 x_j + \sum_{i=1}^{k} \sum_{j=1, i<j}^{k} \beta_{ij} x_i x_j^2 + \sum_{i=1}^{k} \beta_{iii} x_i^3 \quad (2)$$

where $\mathbf{x}$ is the vector of independent variables, f is the output (predicted) function, while β_0, β_i, β_{ii}, β_{iii} and β_{ij} are the coefficients that must be determined through a model fitting process, e.g., using the least squares method.

3.2. Shepard k-Nearest

The SKN algorithm is a combination of two well-known non-parametric deterministic techniques: Shepard's and k-Nearest [24–26]. In this regression method, the impact of the known data points $x_i \subset \Omega$ on a predicted $\mathbf{x}^*$ is controlled by assigning weighting factors, which are inversely proportional to the distance between them. The k-Nearest regression method computes the predicted value $\mathbf{x}^*$ as the weighted average of the k closest to $\mathbf{x}^*$ known data points. This can be written by Eq. 3:

$$f^*_{SKN}(\mathbf{x}^*) = \sum_{i=1}^{k} w_{i,t}(\mathbf{x}^*) y_{i,t} \quad w_{i,t}(\mathbf{x}^*) \in \Re \tag{3}$$

where $w_{i,t}(\mathbf{x}^*)$ denotes the weight assigned to the $t-th$ data point and $y_{i,t}$ is the known dependent value. The weights are defined using Eq. 4:

$$w_{i,t}(\mathbf{x}^*) = \begin{cases} \frac{\|\mathbf{x}^* - \mathbf{x}_{i,t}\|^{-p}}{\sum_{t=1}^{k} \|\mathbf{x}^* - \mathbf{x}_{i,t}\|^{-p}} & if \quad \mathbf{x}^* \neq \mathbf{x}_i \quad \forall t = 1, ..., k \\ 1 & if \quad \mathbf{x}^* = \mathbf{x}_i \end{cases} \tag{4}$$

where p is an arbitrarily chosen parameter. According to Shepard [25], in order to allow the approximation surface to be smooth, the recommended value of this parameter is equal to $p = 2$.

3.3. Gaussian Process

The GP is a non-parametric model, being a collection of random variables, any finite number of which have a joint Gaussian distribution [27]. It is defined by its mean $\mu(\mathbf{x})$ and covariance $k(\mathbf{x}, \mathbf{x}^*)$ functions, according to Eq. 5:

$$f(\mathbf{x}) \sim GP(\mu(\mathbf{x}), k(\mathbf{x}, \mathbf{x}^*)) \tag{5}$$

The former function is frequently taken as zero [28, 29]. The latter, known as the kernel, describes the dependency between the input and the output. In the subsequently described study the squared exponential covariance function was utilized, which for d-dimensional case takes the form of Eq. 6:

$$cov(\mathbf{x}_i, \mathbf{x}_j) = k(\mathbf{x}_i, \mathbf{x}_j) + \sigma_e^2 \delta_{ij} = \sigma_f^2 exp(-\frac{1}{2}(\sum_{d=1}^{D} \frac{(x_{d,i} - x_{d,j})^2}{l_d^2})) + \sigma_e^2 \delta_{ij} \quad i, j = 1, ..., n \tag{6}$$

where σ_f denotes the highest allowable covariance value [30], l_d is the distance parameter, n is the number of known data points, σ_e represents the data noise and δ_{ij} is the Kronecker delta function.

In order to fit the GP model to the training data obtained by the FEM analyses, in the case study presented here, the prediction error was minimized by tuning the σ_f, σ_e and l_d parameters. Despite that computer simulations are fully deterministic and therefore not burden with measurement uncertainty, the error element in the covariance function was not excluded from the computations, in order to prevent GP model overfitting [29].

3.4. Validation of the metamodels

To assure that prediction-based design will not lead to erroneous results, the metamodel should be validated. In the case of deterministic input data, a frequently used metrics for assessing model accuracy is the R^2 (i.e., R-squared) estimator, expressed by Eq. 7 [28]:

$$R^2 = 1 - \frac{\sum_{i=1}^{k}(y_i - f_i)^2}{\sum_{i=1}^{k}(y_i - \bar{y})^2} \cdot 100\% \tag{7}$$

where k is the number of input points y_i, $\bar{y}$ is the mean of all the inputs and f_i denotes the predicted values for the input vectors (i.e., each predicted f_i corresponds to one known y_i). The closer to unity is the R^2 value, the better the metamodel approximates the input data. However, since it is set on the residual vectors, it cannot be used for interpolation metamodeling techniques. For this reason, in the RS validation process described below in this paper, the R^2 measure was used for polynomial and GP surrogates only.

In some cases, however, high value of R^2 can be misleading, showing nearly perfect approximation quality for an over-fitted model. To overcome this problem it is essential to verify the accuracy of a surrogate using different methods, based on statistical estimators [31, 32]. In such cases the assessment of surrogate accuracy is carried out on an additional set of data. The most frequent indices of this type are the maximum absolute error (MAX), the root mean square error (RMSE) and a modification of the latter, denoted as normalized RMSE (NRMSE). The first out of the three, is a local measure of the deviation between the observed and the predicted output values, as described by Eq. 8:

$$MAX = max|y_i - f_i|, \quad i = 1, ..., m \tag{8}$$

where m is the number of elements in a validation data set. In case of iterative RS fitting, this quantitative measure can be used to indicate a region of a design space, which requires sampling refinement.

The RMSE and its more intuitive normalized modification, which expresses RMSE as a percentage of the output data range, can be calculated by using Eq. 9 and Eq. 10, respectively:

$$RMSE = \sqrt{\frac{\sum_{i=1}^{m}(y_i - f_i)^2}{m}}, \quad i = 1, ..., m \tag{9}$$

$$NRMSE = \frac{RMSE}{y_{max} - y_{min}} \cdot 100\% \tag{10}$$

where y_i and f_i denote observed and predicted output data values. The RMSE and NRMSE measures describe quantitatively the overall accuracy of a tested metamodel. As such, these estimators are perceived as global validity measures. Additionally, the NRMSE can be used to compare metamodels of different scales (e.g., gear TE in micrometers and tooth bending stress in megapascals), therefore it is useful in multi-objective optimization problems.

In the RS model fitting presented subsequently, R^2 measure was used for the data points obtained in the DoE, along with RMSE, NRMSE and MAX estimators combined with a validation set of points.

4. Methodology workflow

The workflow of the proposed optimization approach is presented in Fig. 1. The first step is the preparation of the FE model of the gear pairs, which afterwards are subjected to mesh morphing process to allow for micro-geometry modifications of tooth profile. The subsequent step is the generation of the design of experiment (DoE) through a set of individual solutions, which are analyzed later to provide data essential for building appropriate metamodels using GP, 3rd order PL and SKN techniques. In order to select the most accurate data prediction approach for each of the output quantities, an additional set of known data points is used, combined with three accuracy indices: the maximum absolute error (MAX), the normalized root mean square error (NRSME) and, for the surrogates generated using GP and PL approaches, the R-squared (R^2) measure.

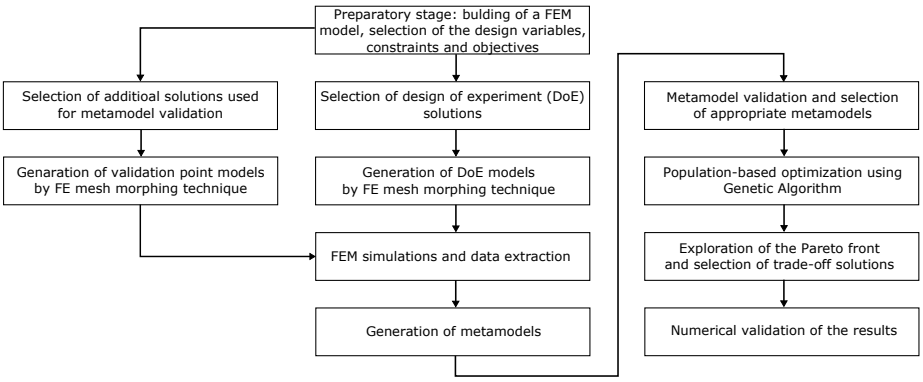

Figure 1: The optimization procedure workflow.

After selecting the most appropriate metamodeling technique for each of the output quantities, the global optimization is performed, using the CEGA algorithm, under constraints related to tooth bending fatigue strength. This results in the formulation of the Pareto front, from which the individuals representing the trade-offs between the objectives are selected manually, based on the foreseen level of improvements that they provide. The last step of the procedure is the numerical validation of the RS-predicted performance of the selected solutions, among which the most suitable one is selected as the final optimization result.

5. Tooth profile modification

Tooth micro-geometry profile modification has a significant impact on the static and dynamic behavior of a geared transmission, as shown in the literature [2–5, 9, 15, 33, 41–43]. Although the most common way of applying micro-geometry modifications is to provide both tip and root relief, researchers observed no substantial difference in the effects of applying both of these modifications or an equivalent tip relief only in micro-geometry of spur gears [8, 33]. For this reason, in the research presented in this paper, we decided to investigate the influence of linear (in the roll distance domain) tip relief only. The two parameters that were used in this study to describe the modification were tip relief depth d and starting radius r_t. The same micro-geometry modifications were applied to the driving and the driven gear. Consequently, only two parameters controlled the modification process, i.e., amplitude and length of tip relief. Figure 2 shows an example of the imposed linear tip relief modification as a function of the roll distance (a) and in the coordinate system of the FE model (b). Part (c) of Fig. 2 presents a comparison between the modified and the original FE meshes.

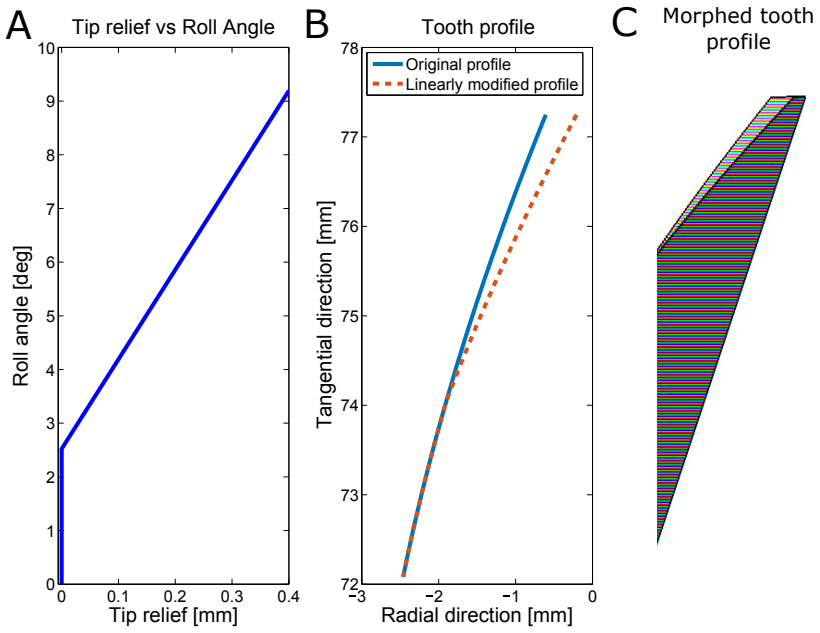

Figure 2: Tip relief deviation from the involute profile calculated in roll angle domain and transformed into nodal coordinates in the FE model for a micro-modified gear with $d = 74.1mm$ and $r_t = 0.4mm$. The roll angle in figure 2a is measured from the initial contact point on the active tooth profile.

The tooth profile modification was carried out on a baseline FE model described above. The gear teeth were modified using the mesh morphing tech-

nique, by moving the so-called handles attached to the tooth profile nodes, as shown in Fig. 3. This technique was utilized in order to maintain the quality of FE elements.

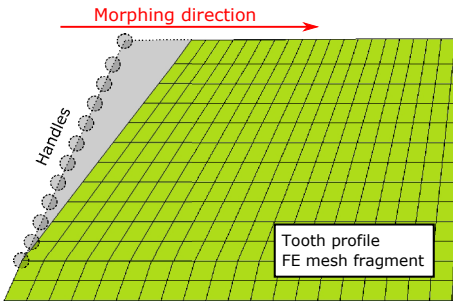

Figure 3: Tip relief imposed by means of the FE mesh morphing technique.

6. FE modeling and analysis of meshing gears under static load

In order to assess the proposed strategy for multi-objective optimization of gear micro-geometry, a pair of identical spur gears was analyzed, for which Tab. 1 summarizes the geometric parameters. Below, we provide a short presentation of the utilized FE model, description of each of the output quantities and their meaning to gear design.

6.1. Gear FE model

The procedure of tooth profile modification was carried out on a the FE model shown in Fig. 4. The gear bodies and teeth were discretized using three-dimensional hexahedral elements, while the shafts were simplified to rigid representations. It is worthy to point out that the region of the gears, in which no contact was expected, was discretized using a coarse FE grid. Conversely, in the case of teeth for which meshing contact was foreseen, smaller elements were used. The size of the FE mesh in contact region was determined using the convergence analysis, which was carried out on a set of models constructed with different FE mesh refinements.

6.2. Static Transmission Error (STE)

In practice, the micro-geometry modifications are applied to gears principally to decrease the STE peak-to-peak value, which is a measure of internal vibration source and, as mentioned in the introduction, is correlated with the dynamic TE [6, 7]. TE is defined by Smith in ref. [33] as 'the difference between the angular position that the output shaft of a drive would occupy if the drive were perfect and the actual position of the output'. The STE can be considered as the TE measured in quasi-static conditions. It is frequently transformed into longitudinal displacement along the line of action and as such expressed by Eq. 11:

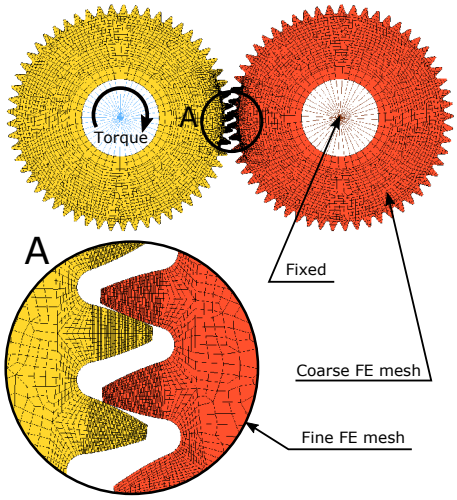

Figure 4: The analyzed FE model of the meshing spur gears.

Table 1: Gear design specifications.

Parameter Name	Value
Number of teeth	57
Normal module	2.60 mm
Normal pressure angle	20 deg
Tip diameter	154.50 mm
Root diameter	141.70 mm
Face width	23 mm
Normal circular teeth thickness at theoretical pitch circle	3.78 mm
Kinematic contact ratio	1.45
Theoretical pitch diameter	148.20 mm
Working center distance	150 mm
Generating tool edge radius coeff.	0.555

$$STE = r_{B1}\Theta_1 - r_{B2}\Theta_2 \tag{11}$$

where r_{B1}, Θ_1, r_{B2} and Θ_2 are the base radii and measured rotation angles for driving and driven gears. The STE is heavily affected by profile reliefs, which, for low loading torque values, can result in the elimination of contact between the teeth in some regions of the meshing cycle. In gears with micro-modified profiles, the STE can be divided into two contributions [34]: the geometric (or rigid) component and the elastic deflection component, as shown in Fig. 5. The former results from free gear rotation which can take place when profile tip relief is used and therefore, when distance between teeth is increased. The latter is caused by gear deflection under load.

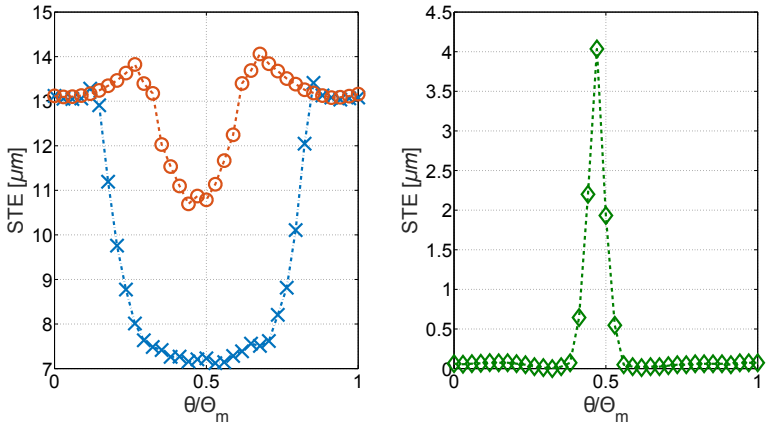

Figure 5: Static transmission error obtained for: a) the unmodified model (blue crosses) and the model after micro-geometry modification with $d = 21\mu m$, r_t=76.19 mm (red circles); b) rigid part of the TE

6.3. FE model convergence analysis

The STE curve quality was used as a measure for FE model mesh convergence analysis. Three models were used to calculate the STE curve along one meshing cycle. The method used for these calculations was based on a series of non-linear static simulations, carried out on the gear pair positioned along the meshing cycle with an angular step equal to $\Delta\theta = 0.21deg$, as described in [35]. Measured along a tooth profile, the three tested element sizes were: 0.07mm, 0.11mm and 0.15mm. In the analysis, the driving gear was loaded by 350Nm torque. The results obtained were compared with one another (Fig. 6), which enabled choosing the optimal FE element size. Based on the obtained data, it was decided to use the 0.11mm FE element size. This value guaranteed good quality results and relatively small number of elements in the FE model, which was equal to 148019, corresponding to 526321 active degrees of freedom.

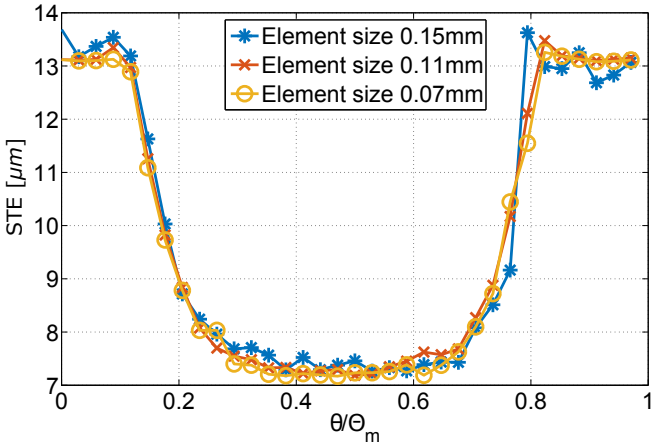

Figure 6: Convergence analysis of the FE model mesh using 350Nm loading torque applied on the driving gear.

6.4. Tooth bending fatigue

Stress generated in the tooth root is often taken as a measure for gear bending fatigue. Root fillet undergoes frequent loading unloading cycle, thus it is prone to this type of failure. The calculation of root fatigue strength requires the estimation of element values of the principal stress tensor, which are subsequently used to assess the fatigue mean and alternate stresses [34]. Combination of these two quantities can be used for assessing the gear material fatigue strength, using the Haigh diagram [40]. In order to understand which side of a tooth undergoes more significant fatigue bending load, the mean and alternate stress computed for contacting and free side of a tooth are compared in Fig. 7.

These values were calculated in the mid-width region of the fillet, which is often chosen for positioning strain gauges in experimental measurements. As it can be deduced from the presented results, due to high cyclic tension loads, the region crucial for bending fatigue is the one on the contact side of the tooth. For this reason, the subsequent computations of fatigue strength were carried out for σ_1 and σ_3 components of the principal stress tensor, evaluated for the root fillet located on the contact tooth side. Figure 8 depicts examples of principal stress history obtained for unmodified and modified gears and expressed in normalized meshing cycle angle $\theta/\Theta m$, where θ is the instantaneous meshing angle and Θ_m denotes total meshing angle. The maximum and minimum values of these quantities for every gear modification pattern were subsequently used for metamodeling and data prediction.

6.5. Contact stress

Contact stress in meshing teeth is calculated on the flank, showing local concentration of internal material pressure. This value is important for gear

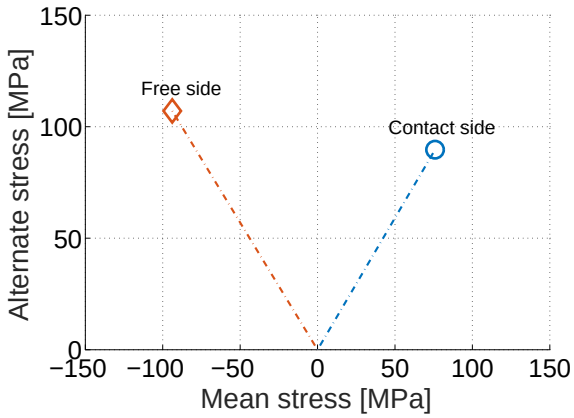

Figure 7: Mean and alternate stress calculated for a tooth root fillet: on the contacting and free tooth flank.

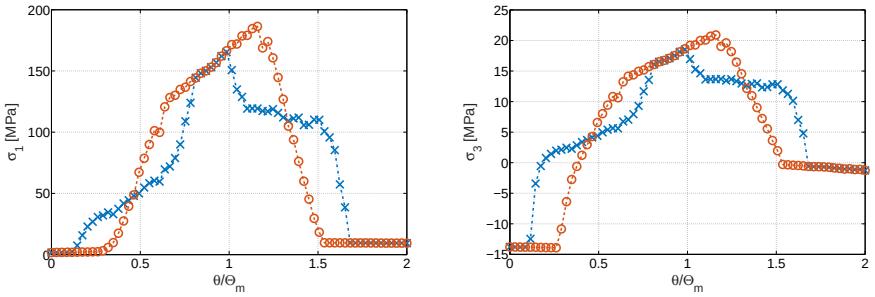

(a) (b)

Figure 8: Bending principal stress history: (a) - σ_1 and (b) - σ_3, for unmodified model (blue crosses) and the model after micro-geometry modification with $d = 21\mu m$, $r_t = 76.19mm$ (red circles). Gears were loaded by a 350Nm torque.

design because it drives the process of tooth surface scuffing and pitting, as discussed in ref. [14, 34]. As the contact pattern and position on the tooth flank is influenced by the micro-geometry modification, this value should be observed and minimized to avoid premature failure of a transmission. Figure 9 depicts examples of maximum contact stress histories in meshing angle domain. As described in [36], maximum values of contact stress is observed when a tooth enter and leave the contact. As seen in the same figure, application of micro-geometry modification can alleviate this unwanted effect (as depicted by red dots in Fig. 9). In the subsequent RS fitting, only the highest calculated value for each micro-geometry modification pattern was considered.

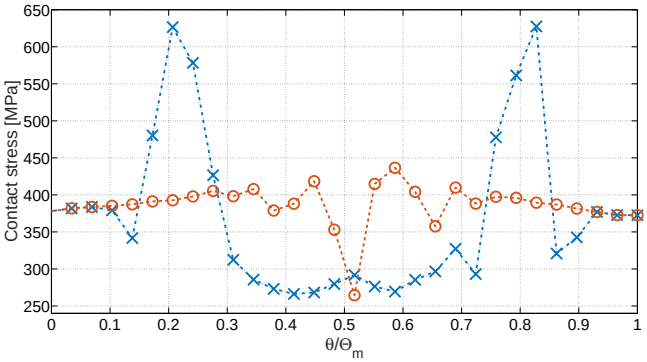

Figure 9: Maximum contact stress values calculated for a unmodified model (blue crosses) and for a model after application of micro-geometry modification with $d = 21\mu m$, $r_t = 76.19mm$ (red circles).

7. Metamodels

The DoE set was formed by using LHS algorithm by selecting 28 individuals. As shown in Fig. 10, the initial set of individual data points was chosen to cover the design domain area spanned over the region limited by the boundary values $r_t \in < 0.00mm, 0.04mm >$ and $r_t \in < 74.10mm, 77.25mm >$, for depth ($d$) and length ($r_t$) of tip micro-geometry modification respectively. Additionally, to preclude infeasible solutions resulting from deep and short reliefs, the design domain was confined by a line passing through the points $(d_1, r_{t,1}) = (0.00mm, 74.10mm)$ and $(d_2, r_{t,2}) = (0.04mm, 75.675mm)$. Furthermore, four corner points were taken under consideration to limit the design domain. This approach resulted in 32 data points obtained by carrying out 31 analyses. The solution positioned in point $(d_1, r_{t,1}) = (0.00mm, 74.10mm)$ was geometrically equal to the one settled in point $(d_3, r_{t,3}) = (0.00mm, 77.25mm)$, i.e., zero-depth tip relief was applied in both cases.

Subsequently, the LHS algorithm was used to select 6 additional points, which were utilized for validation of each metamodel with RMSE and MAX estimators. These points are marked by crosses in Fig. 10.

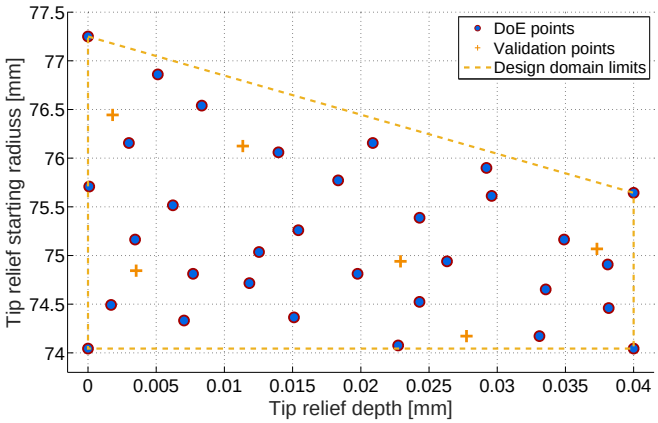

Figure 10: Position of data points calculated in the design domain for RS construction (DoE points) and its validation.

7.1. Construction and validation of metamodels

Using the three mentioned approaches, GP, 3rd order PL and SKN, the data points required for the DoE were obtained for the analyzed gear pair under three different loading torques: 350Nm, 500Nm and 650Nm. The same load values were used to calculate the observed quantity values for the additional validation points, to test the accuracy of the generated metamodels for each loading scenario.

Table 2: Metamodel validation results for 350Nm loading torque.

		STE $[\mu m]$	Contact Stress [MPa]	σ_1 [MPa]	σ_3 [MPa]
PL	$R^2[\%]$	87.7	77.3	83.3	91.0
	$NRMSE[\%]$	10.72	11.13	11.04	9.65
	$MAX\|y_i - f_i\|$	2.99	47.73	5.70	0.03
SKN	$NRMSE[\%]$	9.12	15.85	7.59	4.75
	$MAX\|y_i - f_i\|$	2.09	67.01	3.92	0.02
GP	$R^2[\%]$	99.5	90.2	97.8	88.0
	$NRMSE[\%]$	2.11	7.54	3.99	11.12
	$MAX\|y_i - f_i\|$	0.60	40.91	1.98	0.04

Tables 2-4 describe validation results of the metamodels constructed by using the three selected techniques for each value of applied torque. A detailed analysis of the metamodeling results allowed for selecting the most suitable surrogates for the observed quantities.

Based on this data, the following approximation techniques were chosen for the subsequent optimization procedure: the SKN technique was used for σ_3 calculated for gears under 350Nm torque. The prediction of contact stress

generated on the tooth flanks under the 650Nm torque was done by using the 3rd order polynomial. The values of all the other outputs were predicted using the GP algorithm, which appeared to be the most accurate, according to the metrics used. The NRMSE for all the GP metamodels was below 7.55%, while R2 for residuals was close or above 90%.

Figures 11 and 12 show the selected metamodels representing the objective functions for the subsequent optimization procedure, calculated for different loading torques. It can be seen that the STE and contact stress values vary with the micro-geometry modification in different way. This observation justifies implementation of a multi-objective optimum-search algorithm, for finding a set of design parameters providing improvements in all the observed outputs, simultaneously.

Table 3: Metamodel validation results for 500Nm loading torque.

		STE $[\mu m]$	Contact Stress [MPa]	σ_1 [MPa]	σ_3 [MPa]
PL	$R^2[\%]$	54	94	88	74.0
	$NRMSE[\%]$	18.74	8.75	7.69	9.31
	$MAX\|y_i - f_i\|$	3.81	44.72	6.14	0.03
SKN	$NRMSE[\%]$	7.55	12.81	5.63	11.70
	$MAX\|y_i - f_i\|$	1.59	95.26	3.51	0.04
GP	$R^2[\%]$	99	98	95	86
	$NRMSE[\%]$	2.75	4.77	4.65	6.95
	$MAX\|y_i - f_i\|$	0.45	39.62	3.58	0.03

Table 4: Metamodel validation results for 650Nm loading torque.

		STE $[\mu m]$	Contact Stress [MPa]	σ_1 [MPa]	σ_3 [MPa]
PL	$R^2[\%]$	45	98	98	68
	$NRMSE[\%]$	22.89	4.55	3.49	9.97
	$MAX\|y_i - f_i\|$	4.57	44.79	2.90	0.03
SKN	$NRMSE[\%]$	9.59	9.56	3.67	10.29
	$MAX\|y_i - f_i\|$	1.46	104.67	2.44	0.03
GP	$R^2[\%]$	99	98	99	78
	$NRMSE[\%]$	2.72	4.97	2.43	8.12
	$MAX\|y_i - f_i\|$	0.56	41.63	1.94	0.03

The analysis of Fig. 11 reveals that the depth of tip relief, which results in minimal STE value, increases with the loading torque. It can be also seen that for unmodified tooth profile, i.e., for tip relief equal to zero, the peak-to-peak values of the STE are the lowest for the lowest external load. Such a behavior mimicked by the constructed metamodels is consistent with the expected behavior of the analyzed transmission, considering that the elastic tooth deflection, which causes STE in nominal gears, increases with the loading torque value.

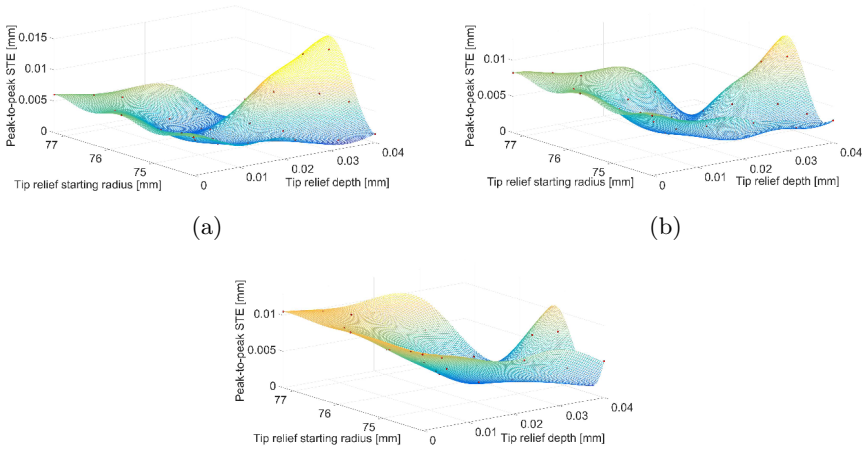

Figure 11: The GP metamodels for STE prediction under: (a) 350Nm, (b) 500Nm and (c) 650Nm torque.

The peak contact stress shown in Fig. 12 is the highest for all the tested loading scenarios for the gears without tip modifications. As discussed in ref. [36, 37], this phenomenon is driven by the fact that, when no relief is applied to the tooth tip, the contact appears on the tooth edge. An optimal value of tip micro-geometry modification allows avoiding this situation, accommodating tooth elastic deflection. As shown in Fig. 11, for each loading torque, a separate set of optimal parameters for micro-geometry tip modification can be found. Although it is less evident compared with the STE output, also in the case of gear contact stress minimization, the region of optimal micro-geometry modification is shifted towards higher values of tip relief, when the input torque is increased.

8. Definition of the optimization problem

The definition of the optimization process starts with the formulation of the objectives and constraints. In the optimization problem addressed in this work, the STE peak-to-peak value and the peak value of the contact stress were calculated for each set of modified gears and represented the objectives. The calculation of the STE was based on Eq. 11.

The peak value of the contact stress was derived directly from the results of the nonlinear statics FEM analyses in the form of Huber - von Mises Hencky reduced stress [37, 38].

8.1. Correlation between the objective functions

The relationships between the observed objective functions were studied using linear Pearson correlation factors. Figure 13 presents the dependencies for

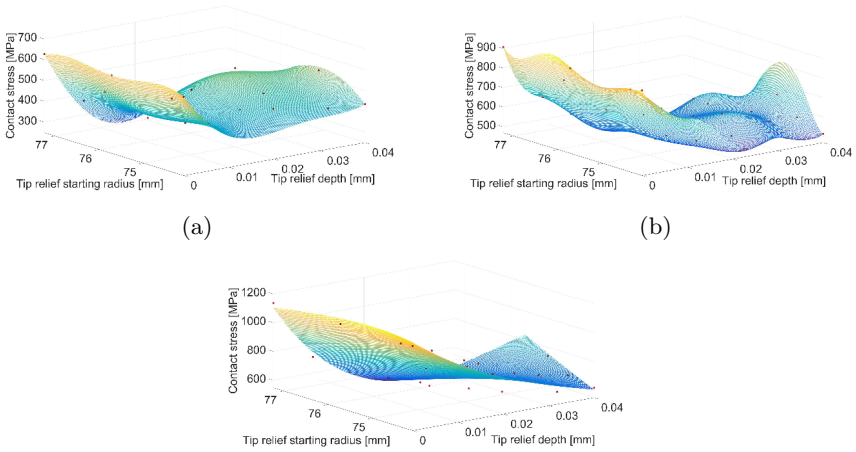

Figure 12: The GP (a and b) and PL (c) metamodels for peak contact stress prediction under: (a) 350Nm, (b) 500Nm and (c) 650Nm torque.

the pairs of selected outputs.

Given two data sets, X and Y, the Pearson correlation coefficient, often denoted as $\rho_{x,y}$, takes values from $< -1; 1 >$ and is calculated using Eq. 12:

$$\rho_{x,y} = \frac{\sum_{i=1}^{n}(x_i - \bar{x})(y_i - \bar{y})}{\sqrt{\sum_{i=1}^{n}(x_i - \bar{x})^2}\sqrt{\sum_{i=1}^{n}(y_i - \bar{y})^2}} \tag{12}$$

where x_i and y_i denote consecutive samples from X and Y, while $\bar{x}$ and $\bar{y}$ are the arithmetic mean values of the two sets. The closer to 1 is the value of this coefficient, the higher degree of positive linear dependency is observed between the variables (i.e., x_i and y_i behave similarly). Conversely, if the value of $\rho_{x,y}$ is close to -1, an inverted linear dependency is observed between x_i and y_i, which is sometimes referred as anti-correlation [39]. When the discussed factor $\rho_{x,y}$ is close to zero, lack of linear dependency between two tested data sets is detected. Using this notation, the Pearson correlation factors were calculated for every pair of objective values in the datasets obtained through FEM analysis in the DoE.

The histograms on the diagonal of the matrix presented in Fig. 13 show the distribution of the analyzed data within the range between minimum and maximum values. All the histograms were created by dividing the total range into ten equally spaced bins. Below the main diagonal, the scatter charts present the distribution of the obtained data in the two-objective space. The solid line on each chart represents the regression line obtained by least square technique, which shows the rate of change between the variables. The calculated correlation coefficients are presented as bar charts above the main diagonal.

It can be seen that none of the analyzed objective pairs are strictly contra-

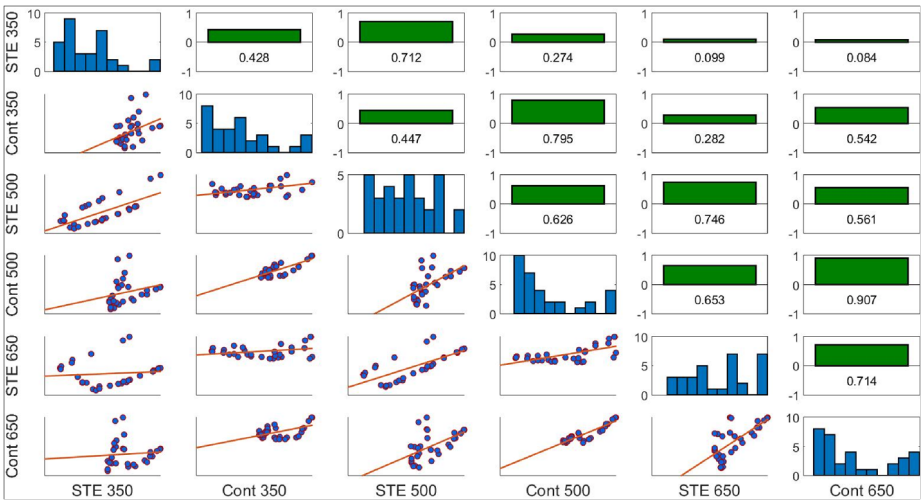

Figure 13: Correlation matrix calculated for the objective functions (STE and Cont stand for static transmission error and contact stress, respectively. The subsequent numerical value indicates the loading torque).

dictory, i.e., no negative correlation was found. However, high $\rho_{x,y}$ was calculated only between contact stress values obtained for gear pair operating under 500Nm and 650Nm torques, for which $\rho_{x,y} = 0.907$. Relatively strong dependencies were also obtained between the corresponding quantities for different torques, i.e., between STEs calculated for 350Nm and 500Nm torques, STEs between 500Nm and 650Nm. Similar observations can be made in the case of the contact stress obtained for different torque levels. These results confirm the deductions achieved from visual inspection of the metamodels shape: the region where the global minimum for each objective function is located was shifted towards greater tip relief for higher values of loading torque. However, it should be also noted that not all of the responses are closely related: 6 calculated correlation coefficients took values below 0.5, which can be perceived as lack of strict connection between these output values.

8.2. Optimization constraints

In operational conditions, each tooth undergoes one loading-unloading cycle for every full rotation of a gear. To prevent gear train premature damage, tooth bending fatigue strength should be controlled when micro-geometry modifications are applied. This is because incautious tooth shape modification can excessively deteriorate this parameter. In typical applications, fatigue loading cycles play a major role for gear endurance.

In order to secure a sufficient bending fatigue resistance of the modified gears, a suitable constraint was defined for the optimization process. Based on the principal stress tensor elements σ_1 and σ_3 extracted from FEM analyses

results, a mean σ_m and alternate σ_a stress are calculated according to Eq. 13 and Eq. 14:

$$\sigma_m = \frac{max(\sigma_1) + min(\sigma_3)}{2} \tag{13}$$

$$\sigma_a = \frac{max(\sigma_1) - min(\sigma_3)}{2} \tag{14}$$

where $max(\sigma_1)$ and $min(\sigma_3)$ denote maximum and minimum value of the selected principal stress tensor elements. Using the Soderberg fatigue diagram presented in Fig. 14, these two quantities can be used to assess the fatigue performance of the analyzed gears. In the presented case, hardening 16MnCr5 steel is assumed as gear material, with yield tensile strength $S_{yt} = 490MPa$ and fatigue strength $S_e = 450MPa$. Using these two values, the fatigue safety factor can be computed as described by Eq. 15:

$$n = \frac{S_e S_{yt}}{\sigma_a S_{yt} + \sigma_m S_e} \tag{15}$$

where n is a fatigue safety factor, describing the position of a point (σ_m, σ_a) compare with Fig. 14 - with respect to the limiting Soderberg line [40]. The constraint used in the presented optimization case, which is enforced in all the loading scenarios, is given by Eq. 16:

$$n \geq 1.5 \tag{16}$$

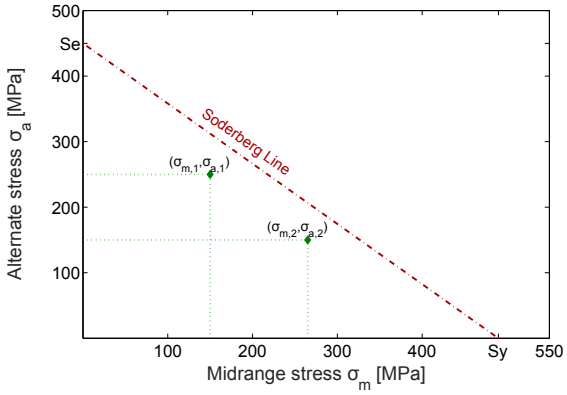

Figure 14: Soderberg line for 16MnCr5 steel, with two sample ($\sigma_{m,i}$, $\sigma_{a,i}$) points describing material fatigue strength.

9. Optimization results

The optimization was carried out using the controlled elitist genetic algorithm, with the following parameters: generation size 100, maximum number of generations 5000, crossover probability 0.85. The stopping criteria were set to reaching either the highest specified number of generations or an excessively small improvements in the best fitness function. During the optimization, it appeared that the first criterion was reached and the process was stopped due to this limitation.

The optimization algorithm found a set of Pareto-optimal solutions, within which three trade-offs were chosen manually, for further testing. These individuals, indicated in Tab. 5 as Sol1, Sol2 and Sol3, were selected based on the level of improvement that they provided in all the objective functions, and because they fulfilled the requirements imposed by the constraint functions. Subsequently, an FE model was built for each of the chosen individuals, in order to carry out numerical validation of metamodel-based predictions. Tables 6-8 present the outcome of this process, comparing the obtained results with the equivalent data for the baseline model.

Table 5: Selected Pareto-optimal solutions.

Solution id	Modifications	
	Depth $[\mu m]$	Starting radius $[mm]$
Sol1	16.3	74.134
Sol2	15.4	74.402
Sol3	13.4	74.190

Table 6: Predicted and FE-derived results for the selected Pareto-optimal solutions for 350Nm torque.

		STE $[\mu m]$	Contact Stress $[MPa]$	Fatigue Safety Coeff.
Unmodified Model	FEM-based	6.078	626.7	2.82
Sol1	Predicted	3.436	374.0	2.770
	FEM-based	3.542	388.6	2.723
Sol2	Predicted	2.473	397.3	2.728
	FEM-based	2.434	389.8	2.729
Sol3	Predicted	3.168	383.4	2.791
	FEM-based	3.775	397.3	2.755

As shown in Tab. 6-8, the numerical validation confirmed that application of the micro-geometry modifications indicated by the optimization algorithm resulted in improvements in all of the specified objective functions. Furthermore, the fatigue safety constraints were satisfied in all the tested cases. The relative prediction error expressed as the difference between the value indicated

Table 7: Predicted and FE-derived results for the selected Pareto-optimal solutions for 500Nm torque.

		STE $[\mu m]$	Contact Stress $[MPa]$	Fatigue Safety Coeff.
Unmodified Model	FEM-based	8.276	907.3	2.04
Sol1	Predicted	6.079	621.3	1.956
	FEM-based	5.689	619.2	1.963
Sol2	Predicted	4.510	558.6	1.946
	FEM-based	4.462	556.2	1.946
Sol3	Predicted	6.057	661.3	1.972
	FEM-based	5.930	667.0	1.987

Table 8: Predicted and FE-derived results for the selected Pareto-optimal solutions for 650Nm torque.

		STE $[\mu m]$	Contact Stress $[MPa]$	Fatigue Safety Coeff.
Unmodified Model	FEM-based	10.527	1136.0	1.61
Sol1	Predicted	7.574	850.5	1.594
	FEM-based	7.960	927.5	1.566
Sol2	Predicted	6.525	838.8	1.562
	FEM-based	6.670	867.4	1.562
Sol3	Predicted	7.930	889.1	1.602
	FEM-based	8.162	950.5	1.579

by metamodel and the one obtained using a FEM analysis, was calculated using Eq. 17:

$$\epsilon_{rel} = \frac{|y_{FE} - y^*|}{y_{FE}} \cdot 100\% \tag{17}$$

where y_{FE} and y^* are the FE-derived and the metamodel-predicted values of a response, respectively. As it can be seen in Fig. 15, all but one error values are below 8.50%, which is in line with the metamodel accuracy discussed previously.

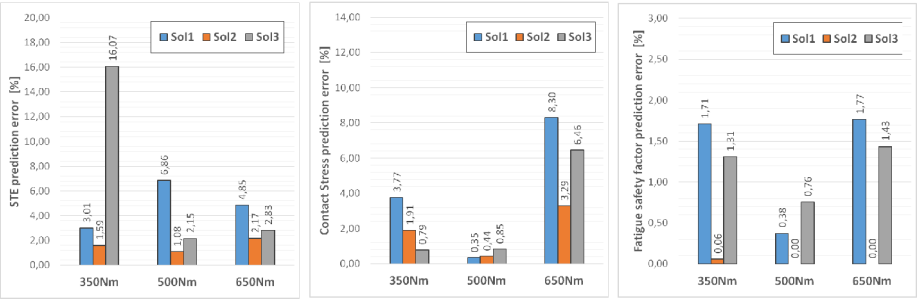

Figure 15: Objective functions and constraints relative prediction error.

With the aim of assessing the quality of each quasi-optimal solution, a performance index is defined for each optimization objective by Eq. 18:

$$\vartheta_{obj} = (\frac{1 - y_{FE}}{y_{base}}) \cdot 100\% \tag{18}$$

where ϑ_{obj} is a relative improvement in an objective function, while y_{base} denotes a baseline value of the corresponding, numerically derived y_{FE} objective for the modified model.

It can be observed in Fig. 16-18 that the application of the micro-geometry modifications according to solution Sol2 resulted in a reduction ϑ_{obj} for all of the objective functions in the range 23.64% - 59.97%. Because of the superior characteristics, this solution is then identified as the final, optimal modification.

10. Conclusions

The paper presents an RS-based approach to optimization of gears, using tooth profile micro-geometry modification as decision variables. This metamodel-based approach allows testing a large number of possible gear tooth modification by a population-based optimum search algorithm, with relatively small computational expense. Through its implementation to gear design process, it is possible to find improvements in multiple design targets simultaneously. Due to strong nonlinearity of this type of design problems, meeting this requirement would be difficult using the manual trial-and-error approach or classical, gradient-based optimization techniques.

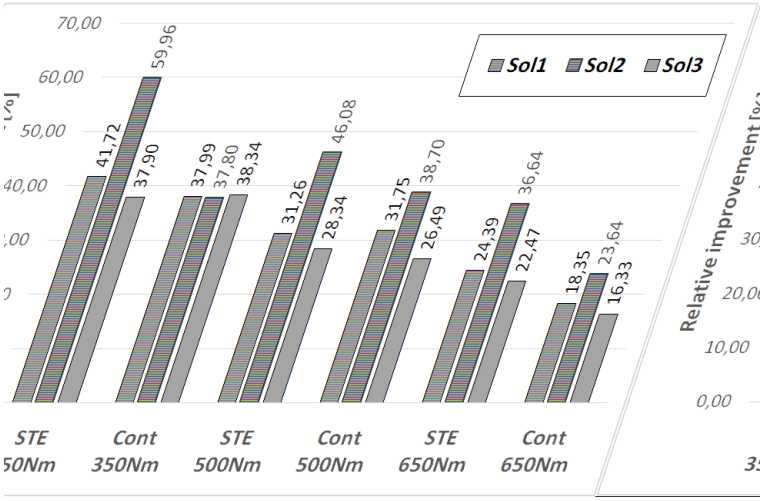

Figure 16: Relative improvements obtained for the analyzed case study.

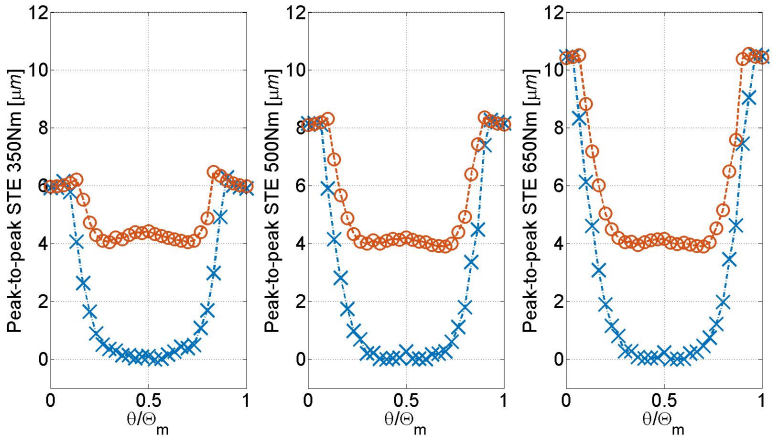

Figure 17: Comparison of STE curves for the unmodified gear (blue crosses) and the quasi-optimal solution Sol2 (red circles).

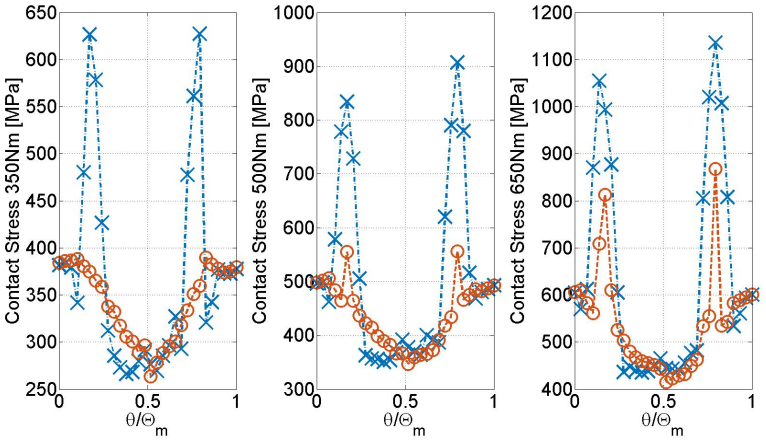

Figure 18: Comparison of Contact Stress history curves for the unmodified gear (blue crosses) and the quasi-optimal solution Sol2 (red circles).

In order to show the usefulness and applicability of the proposed technique, it was successfully implemented to solve the problem of improving transmission error and strength in a pair of identical spur gears, loaded by different torque values. In order to decrease the computational effort associated with testing numerous candidate solutions, metamodeling techniques were used to approximate the data obtained through FE simulations in the DoE phase. Subsequently, the surrogates were used in combination with the population-based CEGA optimization algorithm to find a set of quasi-optimal solutions among 5000 population generations, each consisting of 100 individuals. The final, Pareto-optimal micro-geometry modification pattern was selected manually, based on the improvements provided with respect to the performance of the baseline gear model.

The presented optimization methodology can be used in the gear development process, as an efficient tool for supporting design decisions and helping to achieve the desired characteristics.

11. Acknowledgments

The research leading to these results has received funding from the People Programme (Marie Curie Actions) of the European Union's Seventh Framework Programme FP7/2007-2013/ under REA grant agreement no. 324336 DEMETRA: Design of Mechanical Transmissions: Efficiency, Noise and Durability Optimization.

12. References

[1] Litvin, F. L., & Fuentes, A. (2004). Gear geometry and applied theory. Cambridge University Press.

[2] Artoni, A., Guiggiani, M., Kahraman, A.,& Harianto, J. (2013). Robust Optimization of Cylindrical Gear Tooth Surface Modifications Within Ranges of Torque and Misalignments. Journal of Mechanical Design, 135(12).

[3] Harianto, J., & Houser, D. R. (2007, January). A methodology for obtaining optimum gear tooth micro-topographies for noise and stress minimization over a broad operating torque range. In ASME 2007 International Design Engineering Technical Conferences and Computers and Information in Engineering Conference (pp. 289-303). American Society of Mechanical Engineers.

[4] Artoni, A., Gabiccini, M., Guiggiani, M., & Kahraman, A. (2011). Multi-objective ease-off optimization of hypoid gears for their efficiency, noise, and durability performances. Journal of Mechanical Design, 133(12).

[5] Bonori, G., Barbieri, M., & Pellicano, F. (2008). Optimum profile modifications of spur gears by means of genetic algorithms. Journal of sound and vibration, 313(3), 603-616.

[6] Parker, R. G., Agashe, V., & Vijayakar, S. M. (2000). Dynamic response of a planetary gear system using a finite element/contact mechanics model. Journal of Mechanical Design, 122(3), 304-310.

[7] Cai Yurong, & Hayashi Teru. (1992). Optimum modification of tooth profile for a pair of spur gears to make its rotational vibration equal zero. Paper presented at the American Society of Mechanical Engineers, Design Engineering Division (Publication), 453-460.

[8] Faggioni, M., Samani, F. S., Bertacchi, G., & Pellicano, F. (2011). Dynamic optimization of spur gears. Mechanism and machine theory, 46(4), 544-557.

[9] Fernández, A., Iglesias, M., de-Juan, A., Garca, P., Sancibrin, R., & Viadero, F. (2014). Gear transmission dynamic: Effects of tooth profile deviations and support flexibility. Applied Acoustics, 77, 138-149.

[10] Costas, M., Daz, J., Romera, L., & Hernndez, S. (2014). A multi-objective surrogate-based optimization of the crashworthiness of a hybrid impact absorber. International Journal of Mechanical Sciences, 88, 46-54.

[11] Korta, J., Raniolo, R., Danti, M., Kowarska, I., & Uhl, T. (2012). Multi-objective optimization of a car body structure. SAE International Journal of Passenger Cars-Mechanical Systems, 5(3), 1143-1152.

[12] Khuri, A. I., & Mukhopadhyay, S. (2010). Response surface methodology. Wiley Interdisciplinary Reviews: Computational Statistics, 2(2), 128-149.

[13] Myers, W. R., & Montgomery, D. C. (2003). Response surface methodology. Encycl Biopharm Stat, 1, 858-869.

[14] Zhang, G., Wang, G., Li, X., & Ren, Y. (2013). Global optimization of reliability design for large ball mill gear transmission based on the Kriging model and genetic algorithm. Mechanism and Machine Theory, 69, 321-336.

[15] Kayabasi, O., & Erzincanli, F. (2007). Shape optimization of tooth profile of a flexspline for a harmonic drive by finite element modelling. Materials & design, 28(2), 441-447.

[16] Zhang, J., & Guo, F. (2015). Statistical modification analysis of helical planetary gears based on response surface method and Monte Carlo simulation. Chinese Journal of Mechanical Engineering, 28(6), 1194-1203.

[17] Park, C. I. (2010). Multi-objective optimization of the tooth surface in helical gears using design of experiment and the response surface method. Journal of mechanical science and technology, 24(3), 823-829.

[18] Coello, C. A. C., Van Veldhuizen, D. A., & Lamont, G. B. (2002). Evolutionary algorithms for solving multi-objective problems (Vol. 242). New York: Kluwer Academic.

[19] Deb, K., Pratap, A., Agarwal, S., & Meyarivan, T. A. M. T. (2002). A fast and elitist multiobjective genetic algorithm: NSGA-II. Evolutionary Computation, IEEE Transactions on, 6(2), 182-197.

[20] Li, G., Zhang, Z., Sun, G., Xu, F., & Huang, X. (2014). Crushing analysis and multiobjective optimization for functionally graded foam-filled tubes under multiple load cases. International Journal of Mechanical Sciences, 89, 439-452.

[21] Korta, J., & Uhl, T. (2013). Multi-material design optimization of a bus body structure. Journal of KONES, 20.

[22] Deb, K., & Goel, T. (2001, March). Controlled elitist non-dominated sorting genetic algorithms for better convergence. In Evolutionary multi-criterion optimization (pp. 67-81). Springer Berlin Heidelberg.

[23] McKay, M. D., Beckman, R. J., & Conover, W. J. (1979). Comparison of three methods for selecting values of input variables in the analysis of output from a computer code. Technometrics, 21(2), 239-245.

[24] Cavazzuti, M. (2012). Optimization Methods: From Theory to Design Scientific and Technological Aspects in Mechanics. Springer Science & Business Media.

[25] Shepard, D. (1968, January). A two-dimensional interpolation function for irregularly-spaced data. In Proceedings of the 1968 23rd ACM national conference, 517-524.

[26] Gholipour, Y., Shahbazi, M. M., & Behnia, A. R. A. S. H. (2013). An improved version of Inverse Distance Weighting metamodel assisted Harmony Search algorithm for truss design optimization. Latin American Journal of Solids and Structures, 10(2), 283-300.

[27] Williams, C. K., & Rasmussen, C. E. (2006). Gaussian processes for machine learning. the MIT Press, 2(3), 4.

[28] Simpson, T. W., Poplinski, J. D., Koch, P. N., & Allen, J. K. (2001). Metamodels for computer-based engineering design: survey and recommendations. Engineering with computers, 17(2), 129-150.

[29] Andrianakis, I., & Challenor, P. G. (2012). The effect of the nugget on Gaussian process emulators of computer models. Computational Statistics & Data Analysis, 56(12), 4215-4228.

[30] Ebden, M. (2008). Gaussian processes for regression: A quick introduction. The Website of Robotics Research Group in Department on Engineering Science, University of Oxford.

[31] Meckesheimer, M., Booker, A. J., Barton, R. R., & Simpson, T. W. (2002). Computationally inexpensive metamodel assessment strategies. AIAA journal, 40(10), 2053-2060.

[32] Wang, G. G., & Shan, S. (2007). Review of metamodeling techniques in support of engineering design optimization. Journal of Mechanical Design, 129(4), 370-380.

[33] Smith, J. D. (2003). Gear noise and vibration. CRC Press.

[34] Barbieri, M., Zippo, A., & Pellicano, F. (2014). Adaptive grid-size finite element modeling of helical gear pairs. Mechanism and Machine Theory, 82, 17-32.

[35] Korta, J., Palermo, A., Mundo, D., Sweiki, S., Combining Finite Element and Multibody Modeling Techniques for Time-Efficient Simulation of Nonlinear Gear Dynamics, In Proceedings of SIMUL 2015 : The Seventh International Conference on Advances in System Simulation, pp. 94-99, November 15 - 20, 2015 - Barcelona, Spain.

[36] Ye, S. Y., & Tsai, S. J. (2016). A computerized method for loaded tooth contact analysis of high-contact-ratio spur gears with or without flank modification considering tip corner contact and shaft misalignment. Mechanism and Machine Theory, 97, 190-214.

[37] Qin, W. J., & Guan, C. Y. (2014). An investigation of contact stresses and crack initiation in spur gears based on finite element dynamics analysis. International Journal of Mechanical Sciences, 83, 96-103.

[38] Hassan, A. R. (2009). Contact stress analysis of spur gear teeth pair. World Academy of Science, Engineering and Technology, 58(1), 597-602.

[39] Dowdy, S., Wearden, S., & Chilko, D. (2011). Statistics for research (Vol. 512). John Wiley & Sons.

[40] Shigley, J. E., Mischke, C. R., & Budynas, R. G. Mechanical engineering design, 2004. JE Shigley, Mechanical engineering design, 7(22), 400-405.

[41] Kolivand, M., & Kahraman, A. (2009). A load distribution model for hypoid gears using ease-off topography and shell theory. Mechanism and Machine Theory, 44(10), 1848-1865.

[42] Gabiccini, M., Bracci, A., & Guiggiani, M. (2010). Robust optimization of the loaded contact pattern in hypoid gears with uncertain misalignments. Journal of Mechanical Design, 132(4).

[43] Mermoz, E., Astoul, J., Sartor, M., Linares, J. M., & Bernard, A. (2013). A new methodology to optimize spiral bevel gear topography. CIRP Annals-Manufacturing Technology, 62(1), 119-122.